Biochimica et Biophysica Acta 1818 (2012) 303–317

Contents lists available at ScienceDirect

Biochimica et Biophysica Acta

journal homepage: www.elsevier.com/locate/bbamem

Coarse grained model for exploring voltage dependent ion channels ☆

Anatoly Dryga, Suman Chakrabarty, Spyridon Vicatos, Arieh Warshel *

Department of Chemistry, University of Southern California, Los Angeles, CA 90089-1062, USA

ARTICLE INFO

Article history:
Received 18 May 2011
Received in revised form 28 July 2011
Accepted 29 July 2011
Available online 5 August 2011

Keywords:
Membrane potential
Kv1.2
Gating charge

ABSTRACT

The relationship between the membrane voltage and the gating of voltage activated ion channels and other systems have been a problem of great current interest. Unfortunately, reliable molecular simulations of external voltage effects present a major challenge, since meaningful converging microscopic simulations are not yet available and macroscopic treatments involve major uncertainties in terms of the dielectric used and other key features. This work extends our coarse grained (CG) model to simulations of membrane/protein systems under external potential. Special attention is devoted to a consistent modeling of the effect of external potential due to the electrodes, emphasizing semimacroscopic description of the electrolytes in the solution regions between the membranes and the electrodes, as well as the coupling between the combined potential from the electrodes plus the electrolytes and the protein ionized groups. We also provide a clear connection to microscopic treatment of the electrolytes and thus can explore possible conceptual problems that are hard to resolve by other current approaches. For example, we obtain a clear description of the charge distribution in the entire electrolyte system, including near the electrodes in membrane/electrodes systems (where continuum models do not seem to provide the relevant results). Furthermore, the present treatment provides an insight on the distribution of the electrolyte charges before and after equilibration across the membrane, and thus on the nature of the gating charge. The different aspects of the model have been carefully validated by considering problems ranging for the simple Debye–Huckel, and the Gouy–Chapman models to the evaluation of the electrolyte distribution between two electrodes, as well as the effect of extending the simulation system by periodic replicas. Overall the clear connection to microscopic descriptions combined with the power of the CG modeling seems to offer a powerful tool for exploring the balance between the protein conformational energy and the interaction with the external potential in voltage activated channels. To illustrate these features we present a preliminary study of the gating charge in the voltage activated Kv1.2 channel, using the actual change in the electrolyte charge distribution rather than the conventional macroscopic estimate. We also discuss other special features of the model, which include the ability to capture the effect of changes in the protonation states of the protein residues during the close to open voltage induced transition. This article is part of a Special Issue entitled: Membrane protein structure and function.

1. Introduction

The detailed relationship between the external voltage and the gating of voltage activated ion channels is a problem of great current interest [1–8]. Unfortunately, despite great progress in structural and biophysical studies [1–3,9,10], we still do not have a clear picture of the corresponding structure–function correlation. Furthermore, although there has been a significant progress in computational modeling of ion channels and even some understanding of ion selectivity [11–19], the understanding of the gating process has been limited. Not only that the exact structural changes have not been elucidated but also the energetics of the conformational transition and the coupling to the external voltage are far from being understood. In fact, despite several attempts to analyze these issues by molecular simulations [20–22] we still do not have clear understanding about the nature of the gating and the corresponding energy balance. That is, the simulation time does not allow for sufficient convergence of the free energy associated with very large conformational changes in such a large protein membrane system. Thus the system does not render itself to conclusive brute force simulations. We believe that at present the best option is to use coarse grained (CG) modeling that uses effective surfaces with much fewer minima and traps than the fully atomistic surface and can capture properly the interplay between the external voltage and the ion channel.

A part of the problem of modeling voltage activated ion channels involves the modeling of the effect of the change of the protein conformation on the ion current. Macroscopic models have studied the

☆ This article is part of a Special Issue entitled: Membrane protein structure and function.

* Corresponding author at: Department of Chemistry, 418 SGM Building, University of Southern California, 3620 McClintock Avenue, Los Angeles, CA 90089-1062, USA. Tel.: +1 213 740 4114; fax: +1 213 740 2701.
E-mail address: warshel@usc.edu (A. Warshel).

0005-2736/$ – see front matter © 2011 Elsevier B.V. All rights reserved.
doi:10.1016/j.bbamem.2011.07.043

nature of the ion current in the open channel, but the corresponding relationship to the actual protein structure has not been completely clear. Attempts to do so with microscopic models have resulted in free energy profiles for a single ion transfer and some information on multiple ion transfer [14–16]. However, the overall selectivity current has not been reproduced by any microscopic model and the nature of the selectivity has not been properly evaluated. At present it seems to us that semimacroscopic studies with a realistic electrostatic treatment have provided arguably the most effective way for exploring multi-ion current [17] and providing a probable explanation for the origin of the observed selectivity (attributing it in part to the change in the effective ion–ion repulsion) see [11]. As far as the effect of moving to the closed structure is concerned, to the best of our knowledge the first calculation of the energetics of ion transfer in the closed channel has been reported in the semimacroscopic model of [17] (who has noted that the profile for the KcsA channel corresponds to a closed channel).

Now, despite the relative progress in modeling ion current, the situation is much less promising in studies of the effect of the external potential. That is, there has been interesting Poisson–Boltzmann (PB) macroscopic studies that evaluated the gating charges [23], but the results reflect a macroscopic perspective that may lead to traps as was the case in early studies of electrostatic effects in proteins (see review in [24]). Furthermore, although there are recent microscopic attempts [20], they are either based on assuming a linear potential in the protein membrane region, or on free energy calculations that are unlikely to provide fully convergent results due both to the challenge of obtaining stable solvation free energies in protein interiors and the difficulties in capturing the response of the ionic atmosphere by microscopic simulations (see discussion in Section 3).

As stated above, another major challenge in the field is the evaluation of the energetics of the conformational changes of the channel upon voltage activation. Here the application of brute force microscopic simulations is unlikely to provide converging results of the relevant potential of mean force (PMF) in the near future.

In view of the above challenges it seems to us that CG models provide one of the best option for progressing in this field. Thus we have developed and refined in this work a CG model for simulations of membrane proteins in the presence of external potential (electrodes) and electrolyte solution. This includes the development of a semimacroscopic way for modeling the electrolyte solution between the membrane and the electrodes. Special emphasis is dedicated to a consistent modeling of the effect of external potential, focusing on a realistic description of the electrolytes in the solution regions between the membrane and the electrodes, as well as the coupling between the combined potential from the electrodes plus the electrolyte and the protein ionized groups. The model provides a clear connection to the fully microscopic treatment of the electrolytes and thus allows us to explore possible conceptual problems that are hard to resolve by other approaches. This includes the ability to obtain a clear description of the electrolyte charge distribution in systems that contains the membrane and electrodes (including near the electrodes, where continuum models do not seem to provide the relevant result). Furthermore, the model allows us to evaluate the distribution of the electrolytes before and after the equilibration between both sides of the membrane, and thus the nature of the gating current. The clear connection to the microscopic description, combined with the power of the CG modeling, offers a powerful tool for exploring the balance between the protein conformational energy and the interaction with the external potential in voltage activated channels. This tool is validated here on several levels and is also used to explore some key features of the Kv1.2 voltage activated channel.

2. Methods

Our general strategy involves refinement of our recently developed CG model and the extension of this model to incorporate the electrodes/electrolytes components in the simulation of the protein/membrane system. The main features of the model are described below.

2.1. General features of the coarse grained (CG) model

The present work uses a CG model that describes the main chains by an explicit model and the side chains by a simplified united atom model. This CG model, which is a modified version of the model used in our recent works [25–27], provides a more advanced treatment of the electrostatic effects than most current CG models. Our model expresses the overall free energy (in kcal/mol) as:

$$\Delta G_{total} = \Delta G_{main} + \Delta G_{main,side} + \Delta G_{side}. \quad (1)$$

The main chain atoms are represented explicitly with implicit solvent treatment, while the main-side interaction involves van der Waals and screened electrostatic terms [26]. The major and most relevant part of our CG treatment comes from the ΔG_{side} term, which is given by:

$$\Delta G_{side} = \Delta G_{side}^{vdw} + \Delta G_{side}^{elec} + \Delta G_{side}^{hyd} \quad (2)$$

where the first term describes the effective van der Waals interactions between simplified side chains and is described in details in ref. [26]. The second term represents the electrostatic interactions between the ionizable residues (see below) and the last term represents the hydrophobic contributions which are not included implicitly in the first term (see below). The ΔG_{side}^{elec} term is given by:

$$\Delta G_{side}^{elec} = -2.3RT \sum_i Q_i \left(pK_{a,i}^{w} - pH \right) + \Delta G_{QQ} + \Delta G^{self,ion} + \Delta G_p^{self} \quad (3)$$

where i runs over the protein ionized residues, $pK_{a,i}^{w}$ is the pK_a of the ith residue in water and Q_i is the charge of the ith residue in the given ionization state. Here "ion" and "p" designate, respectively, ionized and polar residues, where each residue can have only one of these two contributions (note that the polar term has not been used in our previous works). The ΔG_{QQ} term represents the charge–charge interaction free energy, which is given by:

$$\Delta G_{QQ} = 332 \sum_{i<j} \frac{Q_i Q_j}{r_{ij} \varepsilon_{eff}} \quad (4)$$

where the free energy is given in kcal/mol, the charge–charge distances (r) in Å and the charges (Q) in electronic charge units. ε_{eff} is the effective dielectric for charge–charge interaction, which reflects the idea established in many of our earlier works (e.g. refs. [28,29]) that the optimal value of ε_{eff} is large even in protein interiors (namely $\varepsilon_{eff} > 20$). This type of dielectric has been found recently to provide very powerful insight in studies of protein stability (see refs. [28,30]). The ionization state of the protein residues were determined by a Monte Carlo approach of ref. [26] for the given pH.

A key element in our approach is the treatment of the self energy, $\Delta G^{self,ion}$, associated with charging each ionized group in its specific environment. This term is given by

$$\Delta G^{self,ion} = \sum_i \left(U_{np}^{self,ion}\left(N_{np}^i\right) + U_p^{self,ion}\left(N_p^i\right) + U_{mem}^{self,ion}\left(N_{mem}^i\right) \right) \quad (5)$$

where U designates an effective potential and i runs over all ionized residues (designated by "ion"). $U_{np}^{self,ion}$, $U_p^{self,ion}$ and $U_{mem}^{self,ion}$ are the contributions to the self-energy from nonpolar residues, polar residues and membrane grid points, respectively. Here, N_{np}^i, N_p^i and N_{mem}^i are, respectively, the effective number of nonpolar residues, polar residues and membrane atoms in the neighborhood of the ith residue. Note that the nonpolar contribution for the membrane is

taken into account separately in the hydrophobic term (described below).

The empirical functions $U_{np}^{self,ion}$ and $U_{p}^{self,ion}$ are given by

$$U_{np}^{Self,ion} = \begin{cases} B_{np}^{Self,ion} \exp\left[-0.2\left(N_{np}-6\right)^2\right] & 0 < N_{np} \le 6 \\ B_{np}^{Self,ion} & N_{np} > 6 \end{cases} \quad (6)$$

and

$$U_{p}^{Self,ion} = \begin{cases} B_{p}^{Self,ion} \exp\left[-0.2\left(N_{p}-4\right)^2\right] & 0 < N_{p} \le 4 \\ B_{p}^{Self,ion} & N_{p} > 4 \end{cases} . \quad (7)$$

The values of $B_{np}^{self,ion}$ and $B_{p}^{self,ion}$ are taken as 4 and −2 kcal/mol, respectively, based on available experimental data and microscopic simulations. The treatment of U_{mem}^{self} will be described below.

The number of nonpolar residues around the ith ionized residue, N_{np}^{i}, is expressed by the analytical function

$$N_{np}^{i} = \sum_{j} F\left(r_{ij}\right) \quad (8)$$

with

$$F\left(r_{ij}\right) = \begin{cases} 1 & r_{ij} \le r_{np} \\ \exp\left[-6\left(r_{ij}-r_{np}\right)^2\right] & r_{ij} > r_{np} \end{cases} \quad (9)$$

where r_{np} is the cutoff range of nonpolar neighboring residues (the current model uses typically $r_{np}=7$ Å and r_{ij} is the distance between the ionized residue i and nonpolar residue j). The same expression is used for the neighboring polar residues (N_p), where $r_p=7$ Å. This treatment is aimed at capturing the fact that an ionized group has to pay a large energy for moving from water to a nonpolar environment [31,32] and is usually surrounded by polar residues or water molecules [31,33]. It should be mentioned that, due to the way the neighboring residues are calculated, N_{np}^{i} and N_{p}^{i} may not have integer values. The validation of our treatment in proteins is reported in ref. [26].

The membrane is represented by a grid of unified atoms, as we have done in our previous studies since 1989 (e.g. see ref. [34]), and this grid is used in evaluating N_{mem} by the equivalent of Eq. (8). The number of the membrane grid points that are reconsidered as neighbors of a given protein residue is calculated by counting the number of membrane atoms inside a sphere with cut-off radius given by the membrane spacing (D_{mem}) multiplied by 2.05 (namely, $r_{mem}=2.05D_{mem}$). This cut-off radius gives results, which are (almost) independent of the membrane spacing (in the range of 2 to 5 Å). In this way we basically count the number of neighbors in the first two solvation shell of the given residue.

In the case of the membrane it seems essential to include the effect of the electrostatic field from the solvent in the self energy term, whereas in the case of proteins (particularly because of the small value of B_{np}) this was not crucial. More specifically, as is clear from studies of the solvation profile in membrane (e.g. [27]), the self energy depends strongly on the distance from the solvent. One option is use Langevin Dipoles (LD) grid (as we did in our early work [35]) but this would have led to a partial double counting of the self energy penalty in the center of the membrane. Thus we use a $U_{mem}^{self,ion}$ term of the form

$$U_{mem}^{self,ion} = \begin{cases} U_{mem}^{self,ion,0} \exp\left[-((R_{min}-18)/12)^2\right] & R_{min} \le 18 \\ U_{mem}^{self,ion,0} & R_{min} > 18 \end{cases} \quad (10)$$

with

$$U_{mem}^{self,ion,0} = \begin{cases} B_{mem}^{self,ion} \exp[-0.2(N_{mem}-28)] & 0 < N_{mem} \le 28 \\ B_{mem}^{self,ion} & N_{mem} > 28 \end{cases} \quad (11)$$

where R_{min} is the distance to the nearest solvent molecule, which is determined by using the distance to the closest grid point. The interaction with the grid points vanishes continuously when the protein moves to a contact with them (see below). The validation of our treatment in membranes is reported in the SI of [27].

The new term ΔG_{p}^{self} in Eq. (3) is evaluated in the same way as $\Delta G^{self,ion}$ with the $B_{np}^{self,pol}$, $B_{p}^{self,pol}$ and $B_{mem}^{self,pol}$ given in Table 1.

All the above electrostatic treatment involves a self-consistent evaluation of the interdependent self-energy, charge–charge interaction and the external pH (where the ionization state is determined by a Monte Carlo treatment of the energetics of Eq. (3)).

In considering the hydrophobic effect we noted that the corresponding interaction between the protein residues is reflected implicitly in the van der Waals parameters used. However, the corresponding calibration has not been done in a very systematic way in the protein and was not done at all for the membrane model. Thus we considered here a unified treatment of the hydrophobic effect in the membrane and in the protein, adopting the same model used in the self energy calculations, expressing ΔG_{side}^{hyd}

$$\Delta G_{side}^{hyd} = \sum_{i} \left[U_{np}^{hyd}\left(N_{np}^{i}\right) + U_{p}^{hyd}\left(N_{p}^{i}\right) + U_{mem}^{hyd}\left(N_{mem}^{i}\right)\right] \quad (12)$$

where i runs over all *nonpolar* residues and N_{np}^{i} and N_{mem}^{i} are the number of nonpolar residues and membrane atoms within a cutoff range of the i^{th} residue. The functions of U_{np}^{hyd}, U_{p}^{hyd} and U_{mem}^{hyd} are given by the same type of expression as in Eq. (6), where the coefficients, B_{np}^{hyd}, B_{np}^{hyd} and B_{mem}^{hyd}, are given in Table 1.

In order to avoid double counting of the implicit hydrophobic effect of the protein–protein van der Waals interaction we did not include the van der Waals energy of Eq. (2) in our current determination of the total free energy.

A new feature of the model is the use of a membrane grid with continuous forces. This reduces the need for generating a new grid when the protein is displaced or changes its structure. This was done by building an analytically continuous membrane (instead of deleting membrane points, which are in direct contact with the protein). Accounting for the fact that the membrane grid should be deleted upon contact with the protein atoms we have replaced the standard van der Waals interaction between the protein and the membrane by

$$U_{vdw}^{mem} = \sum_{i<j} \left[\frac{A_{ij}}{\left(\alpha + r_{ij}^{6}\right)^2} - \frac{B_{ij}}{\alpha + r_{ij}^{6}}\right] \quad (13)$$

where A_{ij} and B_{ij} are the vdw parameters for the interaction of the ith protein atom and the jth membrane grid point, r_{ij} is the distance between the two atoms, and α is a vdw cutoff parameter. The parameter α has been adjusted for each type of interaction so that the vdw energy will become zero when $r=0$ ($U_{vdw}(r=0,\alpha_0)=0$). The average $\overline{\alpha}$ was then used as a general α in Eq. (13), although this choice led to a slight variation in $U_{vdw}(r=0)$ for different types of interactions (between −0.1 and 0.1 kcal/mol). The parameters A_{ij} and B_{ij} for the interaction between the side chain CG atoms with the membrane grid points were evaluated by using the relations $A_{ij}=4\varepsilon_{ij}^{0}(r_{ij}^{0})^{12}$, $B_{ij}=4\varepsilon_{ij}^{0}(r_{ij}^{0})^{6}$ and $\overline{\alpha}=7452.75$. On the other hand, the interaction of the main chain atoms with the membrane grid points were represented using $A_{ij}=A_iA_j$, $B_{ij}=B_iB_j$ with $\overline{\alpha}=2871.33$. Since the entire membrane grid points were represented by the same parameters we have used only one set of ε^0, r^0 for membrane–side chain interactions and one set of A, B for membrane–main chain interactions (see Table 1). The parameters for

Table 1
CG parameters.[a]

Electrostatic self energy parameters for the ionizable residues							
		$B_p^{self,ion}$	Equation	$B_{np}^{self,ion}$	Equation	$B_{mem}^{self,ion}$	Equation
ARG	Ionizable	−1.0	(7)	4.26	(6)	15.0	(11)
LYS	Ionizable	−1.0	(7)	5.40	(6)	15.0	(11)
GLU	Ionizable	−1.3	(7)	5.14	(6)	15.0	(11)
ASP	Ionizable	−1.3	(7)	3.07	(6)	15.0	(11)
HIS	Ionizable	−1.0	(7)	2.28	(6)	15.0	(11)
HIE	Ionizable	−1.0	(7)	2.28	(6)	15.0	(11)
Electrostatic self energy parameters for the polar residues							
		$B_p^{self,pol}$	Equation	$B_{np}^{self,pol}$	Equation	$B_{mem}^{self,pol}$	Equation
THR	Polar	−0.15	(7)	0.20	(6)	2.0	(11)
SER	Polar	−0.15	(7)	0.20	(6)	2.0	(11)
CYS	Polar	−0.15	(7)	0.20	(6)	2.0	(11)
ASN	Polar	−0.15	(7)	0.20	(6)	2.0	(11)
TYR	Polar	−0.15	(7)	0.20	(6)	2.0	(11)
GLN	Polar	−0.15	(7)	0.20	(6)	2.0	(11)
Hydrophobic parameters[b]							
		B_p^{hyd}	Equation	B_{np}^{hyd}	Equation	B_{mem}^{hyd}	Equation
MET	Hydro	0.5	(7)	−0.18	(6)	−1.0	(11)
ILE	Hydro	0.5	(7)	−0.29	(6)	−1.0	(11)
VAL	Hydro	0.5	(7)	−0.25	(6)	−1.0	(11)
LEU	Hydro	0.5	(7)	−0.29	(6)	−1.0	(11)
ALA	Hydro	0.5	(7)	−0.18	(6)	−1.0	(11)
PRO	Hydro	0.5	(7)	−0.25	(6)	−1.0	(11)
PHE	Hydro	0.5	(7)	−0.3	(6)	−1.0	(11)
TRP	Hydro	0.5	(7)	−0.3	(6)	−1.0	(11)

Parameters for the protein/membrane grid interaction (for side chains)			
	α_0	r_0	ε^0
MEM	7452.75	4.24	0.05

Parameters for the protein/membrane grid interaction (for main chain atoms)			
	α_0	A	B
MEM	2871.33	1956	32

[a] The parameters that are not listed here are given in ref. [26].
[b] The hydrophobic terms were evaluated by starting from the hydrophobic energy in solution (obtained by the ChemSol program [75] and scaling it down). At present we assume that the polar residues do not have hydrophobic contribution.

the protein atoms are given in ref. [26]. To prevent the presence of membrane grid inside channel interiors we eliminate the membrane grid within a cylinder of 4 Å radius around the channel axis.

Another new feature is the description of the effect of zwitterionic membrane head groups. This effect was simulated by placing positive and negative charges on the outer and the subsequent layers of the membrane grid, respectively. The corresponding electrostatic interactions with the protein charges were treated with $\varepsilon_{eff}=20$, which is justified by studies of the field from membrane head groups [36]. However, this element of our model has not been verified in detailed study. Obviously more careful studies are needed to consider recent simulations of the "dipole potential" by Allen and coworkers [37]. Note, however, a careful study of the solvation of hydrophobic ions [38], that were supposed to establish experimentally a large dipole potential, has shown that the conventional interpretation is extremely problematic.

It is also important to emphasize that our current free energy calculations do not involve free energy perturbation (FEP) or potential of mean force (PMF) calculations, since our CG model represents the apparent free energy and the evaluation of the effective potential energy provides a good estimate of the corresponding result obtained with sampling on the same shallow potential energy surface. Note, however, that in principle it is possible to evaluate the PMF of the CG model as we have done in the studies of protein folding problems [35].

2.2. Modeling the electrolytes

A crucial issue in modeling the effect of external potential on membrane proteins is the proper modeling of the effect of the solvent molecules and the bulk ions (electrolytes). The solvent is modeled here implicitly by the above CG model although we could have used a Langevin Dipoles (LD) grid (as done in our earlier work [35]). However as mentioned above, this would have led to a partial double counting of the self energy penalty, as long as we use the treatment of Eq. (2). Thus we still represent here the solvent in an implicit way. However, in evaluating the effect of external potential it is crucial to consider more explicitly the ions in solution at a given ionic strength, and the corresponding treatment of the electrolytes is described below.

In trying to introduce the electrolytes it is important to retain the option of multilevel modeling by describing a key part of the system in a fully discrete model. For example, we can treat the immediate region near the protein by a primitive model with the explicit ions moving by Langevin dynamics treatment [11]. While keeping this option in mind, we will focus below on the next layer of the surrounding, where the electrolytes are described in a simpler way. More specifically, the surrounding electrolytes can be treated macroscopically, going back to the ideas behind the Debye–Huckel (DH) and the Gouy–Chapman (GC) models and subsequent analytical [39,40] and numerical PB models [41,42]. One may also follow the microscopic strategy that was used in Monte Carlo (MC) studies [42–51] and in more recent Langevin Dynamics (LD) and MD studies [52]. Here, however, we try to take a compromise between full MC and grid-type approaches. That is in principle, we would like to start conceptually by placing the ions on grid points (with an assumed separation) and then to use a MC model of type we and others applied in determining the ionization states in proteins [26,53]. However, for practical purposes we will try to introduce some additional simplifications (which can also be removed). The first possible simplification involves creating a grid for the positions of the ions and placing k_1 positive ions and k_2 negative ions on n grid points by a Monte Carlo procedure. This would lead to:

$$\langle q_i\rangle = \frac{\sum_m q_i^{(m)} \exp\left\{-\Delta G^{(m)}\beta\right\}}{\sum_m \exp\left\{-\Delta G^{(m)}\beta\right\}} \tag{14}$$

where $\langle q_i\rangle$ is the average charge at the i-th grid point, m designates the configurations of the charges on the grid points and $\Delta G^{(m)}$ is the free energy of the m-th configuration. The next simplification would be to adopt a approach similar to the Tanford–Roxby model for ionization states in proteins [54], using self-consistent iterations with the potential from the other grid points instead of the MC configurational averaging [55]. This model can be implemented obtained by considering configurations with +1 and 0 charges for the positive ion and −1 and 0 charges for the negative ions. Of course, we can still use a hybrid approach where the nearest neighbors are treated by MC. Next we can further simplify our approach by placing ion pairs on the same grid point (this simplification will be removed in some treatments).

The above approximations lead to the semimacroscopic strategy applied in our previous electrostatic modeling [56], which is similar to the approach introduced originally by Pack and coworkers [57], but retains a much more microscopic view. The grid spacing is taken here as Δ and the volume element $\tau=\Delta^3$, centered at the ith grid point, contains a residual charge (q_i^g) determined by:

$$q_i^g = q_i^+ + q_i^- \tag{15}$$

where

$$q_i^{\pm} = \frac{Z^{\pm}N_{box}^{\pm}e^{\mp\beta\phi_i}}{A^{\pm}} = \frac{Q_{box}^{\pm}e^{\mp\beta\phi_i}}{A^{\pm}} \tag{16}$$

where q_i^+ and q_i^- are, respectively, the positive and negative fractional charges that are assigned to the ith grid point, $z^{\pm}$ is the ion charge of the electrolyte ions in atomic units (namely, ± 1 for the monovalent electrolyte used in our calculations), $N_{box}^{\pm}$ is the total number of cations/anions in the simulation box, $Q_{box}^{\pm}$ is the total charge of cations/anions in the simulation system given by $Q_{box}^{\pm} = z^{\pm} N_{box}^{\pm}$, ϕ_i is the electrostatic potential (times unit charge) at the ith grid point and $\beta = (k_B T)^{-1}$. $A^{\pm}$ is a normalization constant. In the initial step of the calculation $N_{box}^{\pm}$ is obtained as follows for a 1:1 electrolyte.

$$N_{box}^{\pm} = n_{bulk} \tau N_{box}^{grid} \tag{17}$$

where n_{bulk} is number density (number of ions/Å^3), which is connected to the molar concentration (C) by:

$$n_{bulk} = \frac{C}{1666} \tag{18}$$

and N_{box}^{grid} is number of grid points within the simulation box (outside membrane and protein).

To determine the normalization constant $A^{\pm}$, we impose the condition that sum of the charges on all grid points must be equal to the total charge of the system for both cations and anions, i.e. $Q_{box}^{\pm} = \sum_i q_i^{\pm}$. Using Eq. (16) we obtain

$$Q_{box}^{\pm} = \frac{Q_{box}^{\pm} \sum_i e^{\mp \beta \phi_i}}{A^{\pm}} \tag{19}$$

Rearrangement of the above equation gives the normalization constant as:

$$A^{\pm} = \sum_i e^{\mp \beta \phi_i}. \tag{20}$$

Thus, we obtain from Eq. (16):

$$q_i^{\pm} = \frac{Q_{box}^{\pm} e^{\mp \beta \phi_i}}{\sum_i e^{\mp \beta \phi_i}} = \frac{Z^{\pm} N_{box}^{\pm} e^{\mp \beta \phi_i}}{\sum_i e^{\mp \beta \phi_i}}. \tag{21}$$

Our normalization treatment, which is different than the common use of the bulk density, helps to obtain a clearer physical picture (see Section 3.2). However for a very large simulation system and at the limit of $\phi_i \to 0$, we obtain

$$A^{\pm} = \sum_i e^{\mp \beta \phi_i} \to N_{box}^{grid}. \tag{22}$$

Thus, using Eq. (17) we establish that $q_i^{\pm}$ converges to $Z^{\pm} n_{bulk} \tau$ at this limit. An additional discussion of the normalization and related modification will be presented below.

With the above grid charges we can express the potential times unit charge φ_i (which is actually potential of mean force (PMF)) as:

$$\varphi_i = V_i^{ext} + 332 \sum_j \frac{q_j^P}{\varepsilon_{eff}^{gp} r_{ij}} + 332 \sum_{k \neq i} \frac{q_k^g}{\varepsilon^{wat} r_{ik}} + K\left(q_i^+ - q_i^-\right)^2 \tag{23}$$

where, V_i^{ext} represents the external potential on ith grid point, that will be described in Section 2.3. Here, q_j^P is the charge of the jth protein residue (these charges are evaluated by MC procedure described above) and q_k^g is the total charge at the kth grid point given by Eq. (15) (representing the excess net charge of the kth volume element). The last term represents the work invested in polarizing the implicit ion pair on the ith grid point. This is equivalent to the energy of separating the positive and negative part of the implicit ion pair which has been treated explicitly later in this section. We have found K ~ 10 kcal/mol to provide consistent energetics.

The PMF of Eq. (23) does not include the self-energy of the ion since they are the same (for all ions of a given type) in the bulk reference state, but the interaction between the ions in the same grid point are considered in some versions of our model (see below). We also leave out, at present, the $RT \ln(C_i/C_0)$ concentration dependence, which will be important in case of membrane potential with different concentration of electrolytes in the two sides of the membrane.

The long range effect of the regions that are not included in the simulation system is represented by using a partially periodic treatment for computational efficiency. This approach uses multiple replica of the simulation cell along the XY plane with the same box length along the Z direction. These replica grid points are generated explicitly using periodic boundary condition for the nearest neighbor cells (8 cells). The images beyond that are simplified replicas where the charges are averaged on the XY plane and assigned to the central point of every slab along the Z axis, which has coordinate ($N_X L_X$,$N_Y L_Y$,Z), where L_X and L_Y are the simulation box lengths along X and Y axes and N_X and N_Y are integers in the range [−N, N] with $|N_X|, |N_Y| > 1$. Thus the total number of periodic images considered (including the simulation box) is $n_{image} = (2N+1)^2$. The charges are computed only for the primary simulation cell taking into account of the electrostatic energy due to the replicas and then the charges of the replicas are updated in an iterative way. This approach allows us to simulate an effectively large system while minimizing the computational time. In principle we could have used a treatment similar to ref. [58], but we felt more comfortable with the current treatment (of course after properly validating it).

It should be noted that we ignored here the image charge effect, namely the change of the surface charges due to the accumulation of opposing charges near the electrode [59].

The dielectric ε_{eff}^{gp} represents charge–charge dielectric for interaction between the protein and the grid points. This parameter can be approximated by a large number between 40 and 80 or by the function (see ref. [24])

$$\varepsilon_{ij}^{gp} = 1 + 60\left[1 - \exp\left(-0.1 \cdot r_{ij}\right)\right]. \tag{24}$$

At this point we can expand on the normalization by the sum in Eq. (19). As stated above our normalization is different than n_{bulk}, which is the standard normalization in continuum and Poisson–Boltzmann (PB) studies (e.g. [40]), where the charge density is normalized by the bulk density. The difference is expressed basically in the PMF used and in most cases we obtain the same result as that obtained with by PB models for very large simulation system. For such a system we like to retain the option of using a general treatment of a small part of the overall system and thus introduce the following expression:

$$q_i^{\pm} = \frac{Z^{\pm}\left(N_{box}^{\pm} + N_{bulk}^{\pm}\right) e^{\mp \beta \phi_i}}{A^{\pm}} = \frac{\left(Q_{box}^{\pm} + Q_{bulk}^{\pm}\right) e^{\mp \beta \phi_i}}{A^{\pm}}, \tag{25}$$

where the nonexplicit system is represented by a bulk region.

By implementing the normalization condition on the charges both in the simulation system and in the bulk, we obtain

$$A^{\pm} = \left(\sum_{i \in box} e^{\mp \beta \phi_i} + N_{bulk}^{grid} e^{\mp \beta \phi_{bulk}} \right) \tag{26}$$

where the sum in the first term goes over the grid points within the simulation box and N_{bulk}^{grid} is the number of grid points within the bulk system. Here ϕ_{bulk} is a constant potential on the bulk grid points. Thus, we can rewrite Eq. (25) as

$$q_i^{\pm} = \frac{Z^{\pm}\left(N_{box}^{\pm} + N_{bulk}^{\pm}\right) e^{\mp \beta \phi_i}}{\left(\sum_{i \in box} e^{\mp \beta \phi_i} + N_{bulk}^{grid} e^{\mp \beta \phi_{bulk}} \right)}. \tag{27}$$

Using Eq. (17) for the bulk system and going to the limit $\phi_{bulk}\to 0$, and $N^{\pm}_{bulk}\gg N^{\pm}_{box}$ we obtain the standard form:

$$q_i^{\pm}\to Z^{\pm}\left(\frac{N^{\pm}_{bulk}}{N^{grid}_{bulk}}\right)e^{\mp\beta\phi_i}=Z^{\pm}n_{bulk}\tau e^{\mp\beta\phi_i}. \tag{28}$$

However, we feel that the use of our normalization conditions can help to avoid some traps by having a clear microscopic view (see Section 2.3). More discussion of our bulk model is given in Section 3.3.

Our default treatment of using grid points, where each ion pair is placed on a grid point, is similar in spirit to our Langevin diploes (LD) treatment. That is, we are dealing here with simplified explicit ions but we consider only the polarization caused by the change of the equilibrium distribution of the ions from the case without any external potential. Thus for example, the initial distribution of the ions in the system (without an external potential) as well as the corresponding radial distribution function, are not evaluated and the corresponding ion–ion potential in the first solvation cell is taken as the reference potential (see Appendix 5 in [36] for the related case of the LD type models).

In view of the uncertainty associated with the above approach of grouping the charges of the ion pair in each grid point, we have also developed a more microscopic model, with the explicit positions of the positive and negative charges. The corresponding ionic positions are generated by placing the ions in each step along the field from the surrounding, while keeping them at a fixed separation (r_0) which is taken here as 4 Å. Now, the final set of the grid charges is obtained by solving Eq. (16) or (27) and Eq. (23) iteratively, where the free energy of the ionic grid, ΔG_{ig}, is given by:

$$\Delta G_{ig}=332\sum_{i,j}\frac{q_i^g q_j^p}{\varepsilon^{gp}_{eff}r_{ij}}+332\sum_{i>i'}\frac{q_i^g q_{i'}^g}{\varepsilon_{wat}r_{ii'}}+332\sum_i\frac{(q_i^+q_i^--1)}{\varepsilon_{wat}r_0}+\sum_i V_i^{ext}q_i^g. \tag{29}$$

Here the 3rd term represents the interaction between the ion pairs (the equivalent of the last term in Eq. (23)) and is activated only in the version of the model that includes the separated ion pairs. The model with the explicit ion pairs should be particularly useful in future MC simulations.

The evaluation of the residual charges in our model is subjected to the constraint of electroneutrality of the entire protein–membrane system. For example, when the protein charge is $+Q_p$ we move $-Q_p$ charge to the electrolyte system and replace $(Q^+_{box}+Q^+_{bulk})$ in Eq. (25) by $(Q^+_{box}+Q^+_{bulk})-Q_p$. If the bulk is not used we introduce the same correction to the Q^+_{box} in Eq. (21). Note that this modification can be done on either cations or anions since the system will be equilibrated.

2.3. Treating external potentials and membrane potential

One of the major challenges in the present work is the treatment of the membrane potential. Of course, there already exist a number of instructive studies [60–63]. However, these studies have focused primarily on macroscopic descriptions which may be problematic in view of the uncertainties about the dielectric used [24]. This is serious in particular when one uses a dielectric constant of around 2 for the protein and the membrane. Basically using such dielectric constant cannot account for the energetics of ions on the surface of the membrane or in proteins interiors (see e.g. discussion of the helix dipole effect in [24]). Furthermore, macroscopic models may have involve some restrictive assumptions in treating the electrode potential and the electrolytes. Here one may try to use MD simulations with explicit models, but at present we believe that such an approach is not likely to provide converging results, even if one succeeds to generate a few trajectories of the conformational change between the open and close conformations under different external potentials. Probably the most effective treatment should involve the use of CG models with proper electrostatics and with a semimacroscopic ionic grid of the type developed in the previous section.

Our implementation of the CG treatment in models of voltage activated membrane proteins under external potential, starts by considering formally the membrane/protein/water system as a capacitor. That is, in principle we can use the well-known macroscopic capacitor model (e.g. [64,65]), where the external potential induces surface charges (σ_f) whose value will be defined below, and creates the corresponding $\mathbf{D}^0$ as defined below (see Fig. 1).

$$\mathbf{D}^0=4\pi\sigma_f \tag{30}$$

where $\mathbf{D}^0$ is not affected by the medium (the 4π factor is needed in Gaussian units). The determination of the value of $\mathbf{D}^0$ will be considered below. We also have the relationship:

$$\mathbf{E}=\frac{\mathbf{D}^0}{\bar{\varepsilon}}=\mathbf{D}^0-4\pi\mathbf{P} \tag{31}$$

where $\bar{\varepsilon}$ is the macroscopic local dielectric constant (which is not equal to the above ε_{ij}), $\mathbf{E}$ is the macroscopic field and $\mathbf{P}$ is the macroscopic polarization.

The above macroscopic vectors are uniquely related to the corresponding microscopic functions by [36]:

$$\begin{aligned}\mathbf{E}&=\langle\xi\rangle\\ \mathbf{P}&=\langle\mu\rangle\end{aligned} \tag{32}$$

where $\langle\rangle$ designates an average, and $\langle\xi\rangle$ denotes the average over the microscopic field and $\langle\mu\rangle$ denotes the average over the microscopic dipoles.

Our first task is to determine the membrane potential and the electrolytes charges, so we can evaluate the free energy of the protein charges in the presence of this potential. Thus we express the external potential (V^i_{ext}) of Eq. (23) as

$$V^i_{ext}=\int_{Z_0}^{Z_i}D^0_z/\bar{\varepsilon}(Z)dZ \tag{33}$$

where Z_0 is the Z coordinate at the left electrode (in the current work we define the Z coordinate to be increasing from left to right). We can further write

$$\begin{aligned}V^i_{ext}&=D^0_Z(Z_i-Z_0)/\bar{\varepsilon}_{wat},\quad \text{when } Z_i\le Z_1\\ V^i_{ext}&=D^0_Z(Z_1-Z_0)/\bar{\varepsilon}_{wat}+D^0_Z/\bar{\varepsilon}_{loc}(Z_i-Z_1),\quad \text{when } Z_1\le Z_i\le Z_2\\ V^i_{ext}&=D^0_Z(Z_1-Z_0)/\bar{\varepsilon}_{wat}+D^0_Z/\bar{\varepsilon}_{loc}(Z_2-Z_1)+D^0_Z(Z_i-Z_2)/\bar{\varepsilon}_{wat},\quad \text{when } Z_i\ge Z_2\end{aligned} \tag{34}$$

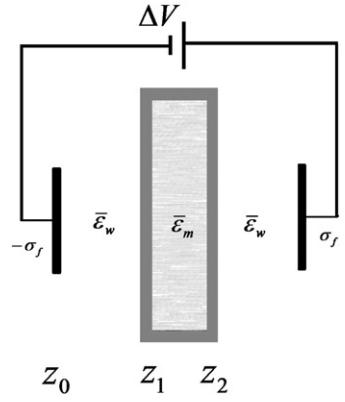

Fig. 1. A schematic representation of the membrane/electrodes system (the membrane can also contain a protein).

here $\bar{\varepsilon}_{wat}$ is the dielectric of the water solution, $\bar{\varepsilon}_{loc}$ is the local dielectric in the membrane/protein system; the Z coordinate of the ith grid point is denoted by Z_i, Z_1 is the point where the membrane (or the protein) has boundary with the left electrolyte solution, Z_2 is the point where the membrane (or the protein) has boundary with the right electrolyte solution (see Fig. 1). The actual value of D_0 is determined by starting with the approximation:

$$D_Z^0 = \frac{V}{\frac{\Delta z_{mem}}{\varepsilon_{mem}} + \frac{\Delta z_{sys} - \Delta z_{mem}}{\varepsilon_{wat}}} \tag{35}$$

where V is the applied potential. We next perform actual calculations and adjust D_0 until the total change of electrolyte potential across the membrane becomes equal to the applied potential.

The problem with the strategy of Eq. (34) is that the potential reflects an infinitely large electrode, while our simulation system is finite (unless we use infinite series like the one used in [46]). Thus the electrolytes will not screen the surface charge from the distant electrode regions (large X and or Y) and the potential V_{ext} will approach infinity at a very large distance from the electrode, reflecting the trend of Eq. (34) for $Z_i < Z_1$ where for finite value of D_0 we will have a very large $(Z_i - Z_0)/\varepsilon_{wat}$.

One way to deal with this problem is to introduce periodicity in the electrolyte system and this strategy will be considered here (see below). The other way is to replace the treatment of Eqs. (33) and (34) by simply generating two finite grids (surfaces) of point charges on the two electrodes. In this approach we use:

$$V_{ext}^i = \sum_j^{N_E} \left(\frac{q_e^{left}}{\varepsilon_{eff} r_{ij}} + \frac{q_e^{right}}{\varepsilon_{eff} r_{ij}} \right) \tag{36}$$

where N_E is number of point charges on the electrode (we place an equal number of points for the left and right electrode), here q_e^{left} and q_e^{right} are the charges of the individual grid points of the electrodes on the right and on the left, taken as equal in the magnitude and opposite in sign. The electrode charge density, σ_f, is determined by requiring that the total potential difference between the electrodes will be equal to the value of the applied potential. This is done by considering a path through the membrane in places where there is no protein (the final potential is path independent) so that we can use Eq. (34) with a simple set of dielectric constants. Although the calculations of the external potential with explicit point charges on the electrode is computationally more demanding than the approach that uses D_0, we only need to calculate this term once. Thus the overall increase in the simulation time is negligible.

It should be noted, with regards to the quasi-periodic treatment, (see section 3.1), that in the direct approach (where $\mathbf{D}^0$ represents an infinite electrode) we only create replicas of the electrolytes boxes, while in the approach that uses explicit surface charges we also replicate the electrode surfaces to the same level of periodicity as the electrolyte box. Further details and validation studies of the long range treatment will be presented in Section 3.1.

In evaluating the energetics of the protein/membrane system in the presence of the electrolytes and the external potential we focus on having a clear microscopic (or semimicroscopic) description. This is done by writing

$$\Delta G_{tot} = \Delta G_{CG} + 332 \sum_{i,j} \frac{q_i^p q_j^g}{\varepsilon_{eff}^{gp} r_{ij}} + 332 \sum_{i,k>j} \frac{q_j^g q_k^g}{\varepsilon_{wat} r_{jk}} + \sum_j V_j^{ext} q_j^p + \sum_i V_i^{ext} q_i^g \tag{37}$$

where the leading term is the free energy of the Eq. (1) in the absence of the external potential and the electrolytes.

The overall simulation system for studies of membrane potential can be described schematically by converting Fig. 1 to the system of Fig. 2. This diagram is related to the normalization concept of Eq. (26). That is, we start with the explicit simulation box that includes the membrane (region I), an optional region (region II) with explicit ions (which has not been considered in the present study) and the explicit grid of the ions (region III). However, now we add a bulk region (region IV), where we require that the electrolyte density will correspond to the bulk density, n_{bulk}, and that the potential will correspond to the electrode potential (V_{bulk}). The assumption that V_{bulk} is equal to the electrode potential is confirmed by our calculations rather than being assumed. The introduction of the bulk region is a way to avoid using enormous grids to span the space between the membranes to the electrodes. The bulk region is coupled to the explicit grid by the fact that the potential of the grid at a sufficient distance from the membrane converges to V_{bulk}, while the ions are allowed to be in the bulk by the use of the normalization condition. The introduction of region IV allows us, in principle, to look for charge accumulation near the electrode. Apparently, the charge distribution in region IV may be different than in the bulk. However, in treatments that do not include region IV explicitly (e.g. in the present case), we consider the charge in the bulk and at the end of the grid region as being somewhere far from the membrane, where the potential reaches a constant value. We may also assume (for the left side) that region IV is the left of the grid, which is in contact with the electrode and the bulk is the region, where the potential start to be constant (this point will be illustrated and discussed using Fig. 2). More details and validation studies will be presented in Section 3.2.

In the practical implementation of the above model we have to take special care of the charges of the ionic atmosphere. This involves, as explained in Section 2.2, satisfaction of the requirement of electroneutrality by balancing the protein charges with the ionic charges in the solution. The placement of the balancing ions can be done in either sides of the membrane, since we allow equilibration of the ions under the applied potential, before we consider the response of the protein and the generation of gating charges (see Section 3.4).

The use of Eq. (34) is valid when we do not have a membrane between the electrodes, as the effective dielectric can be taken as the water dielectric. However, the proper dielectric in the membrane region is less obvious (although the formulation for that system is currently under development looking for strategies that can simplify the electrostatic calculations in systems with several regions with different dielectrics). Thus we prefer to use the $\mathbf{D}^0$ approach (with a periodic electrolyte box) for membrane type systems. In such cases one may wonder what should be the effect of the dielectric that will reproduce the potential from the electrolytes at the membrane. Fortunately, this is not a major problem. That is, the potential in the left side of the membrane, due to the contributions from $\mathbf{D}^0$ and the electrolytes in the right region, is obtained reliably with the water dielectric. At the same time the contributions from the left side of the membrane are independent of the dielectric used for the electrolytes, since the electrolytes near the right electrode and near the right side of the membrane can be viewed as the sources of two opposing vacuum fields that approximately cancel each other. The remaining effect from the right hand side is due to $\mathbf{D}^0$ from the right electrode which is handled consistently through Eq. (34).

3. Results and discussion

3.1. Validation studies

In order to establish the validity of our model we have examined it on several levels. First we have examined our ability to reproduce the Debye–Huckel (DH) analytical approximations for the charge distribution around an ion. More specifically, as in the classical DH model we have represented the ion explicitly by a charge (+1 charge in this case) and the rest of the system was represented by our grid model. In order to get results which are independent of grid spacing and position we have used

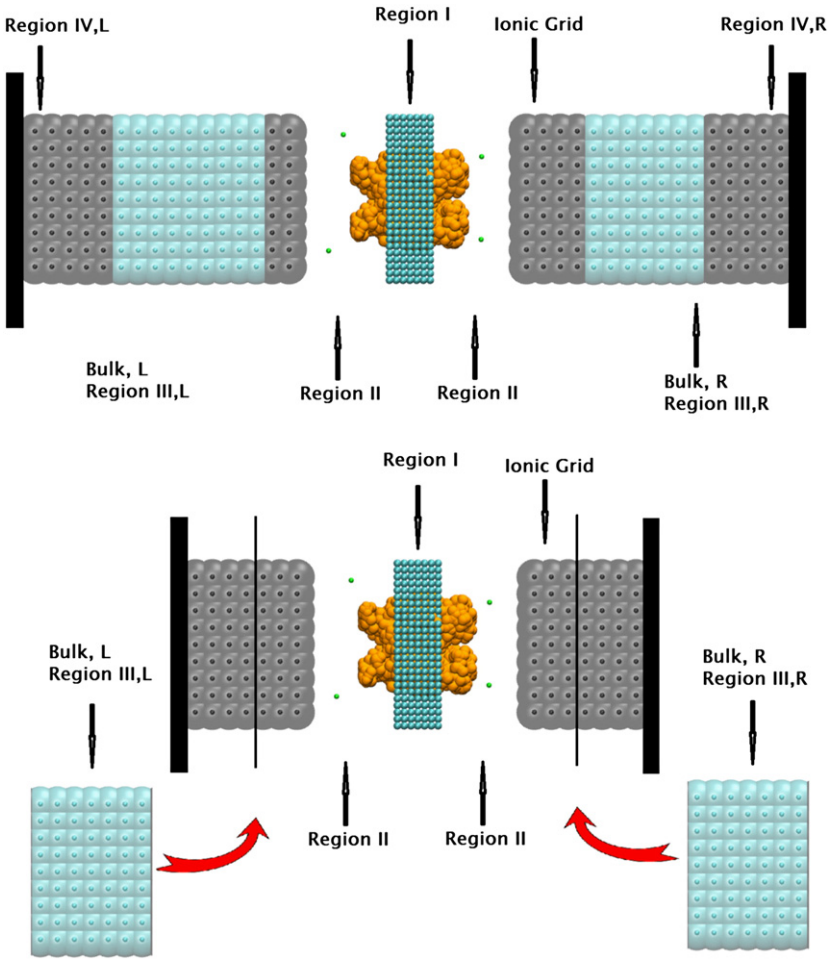

Fig. 2. A schematic description of the treatment of the simulation system. The regions considered are: (a) The protein/membrane system (region I) (b) The region of solution and ions that is treated explicit ions and LD simulation (region II). This region is optional and is not being used in the present study. (c) The region with explicit grid (region III). (d) The bulk region (region IV). (e) The region between the bulk and the electrodes (region V). The indexes L and R stand for the left and right sides respectively.

a similar strategy to that used in our PDLD model, namely generating several shifted and sparse grids (with a spacing of 5 Å between the grid points) and then averaged over the corresponding potential and charge distribution. The simulation results, which are summarized in Fig. 3, have reproduced the DH analytical results quite well. In this respect we must clarify that reproducing the DH results by a semimacroscopic model is very different than reproducing this model by a continuum approximation following the DH assumption (which is rather trivial since the DH is a continuum model). Thus, it is not obvious that our semimacroscopic treatment should reproduce the DH result since it assumes a different normalization and is not a continuum model. Apparently, as seen from Fig. 3 we were indeed able to reproduce the DH results.

Next we explore our ability to model the charge distribution and potential of the electrolytes near a charged surface at a given ionic strength, which is usually described by the Gouy-Chapman (GC) approximation [66]. This type of problem has been the subject of extensive studies including PB, MC and MD [41–50,52]. For this system we have built an explicit sheet of charges on a simulated electrode surface and generated our electrolyte grid on one side of the charged surface. The grid was then allowed to interact with the explicit charges of the electrode as well as with the charges of the different grid points, and the corresponding calculated potential is given in Fig. 4. The calculations have established the ability of our model to reproduce the GC screened electrostatic potential and the condition that the net charge of the electrolytes is equal to the total surface charge. We have also reproduced the correct decay of the potential at the Debye length (30 Å for the system under consideration). More specifically the electrostatic potential becomes zero around 150 Å which corresponds to the analytical result (being approximately equal to five times the Debye length).

We have also explored the performance of our approach on a system composed of two electrodes and electrolytes. The corresponding results (Fig. 5) did provide further major validation, reproducing the trend obtained in MC simulations of the related systems [46].

Next we have explored the performance of our model for a system of the type presented in Fig 2, with two electrodes, electrolyte solution and a neutral membrane. The calculations were done while keeping each side of the membrane electroneutral. This corresponds to application of the potential, while preventing the electrolytes from reaching equilibrium across the membrane (see below). The calculated profiles for the potential along the Z coordinate, where the external potential is 100 mV, are depicted in Fig. 6a. An instructive point that emerges from this figure, is the fact that the application of our model allows us to obtain a reasonable potential around the membrane, even when the electrodes are at a very large distance (this will be impossible without the extra screening effect due to the ions). The calculations demonstrate that the ions in solution provide almost a complete screening to the external potential, which start to increase only when it reaches the membrane boundaries. This behavior is similar to what is expected from macroscopic considerations, but it involves a more challenging treatment since the electrodes are included explicitly here.

We have also evaluated the behavior of the charge distribution and presented in Fig. 6b the corresponding results. Here we obtain results that are different than the conventional PB results [40]. That is, the PB

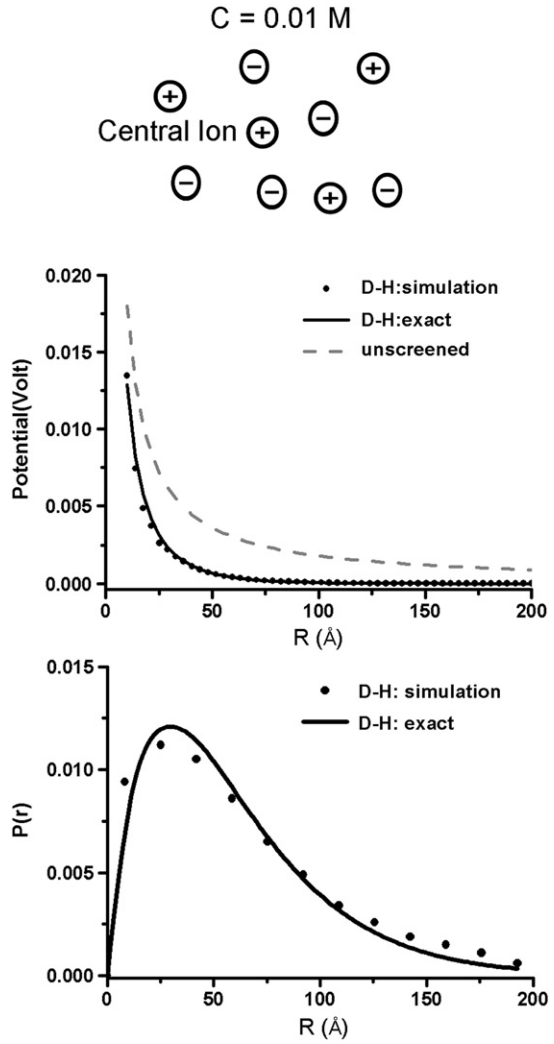

Fig. 3. The potential around a charge obtained by our simulation and by the Debye–Huckel (D–H) theory as well as Coulombic (unscreened) potential.

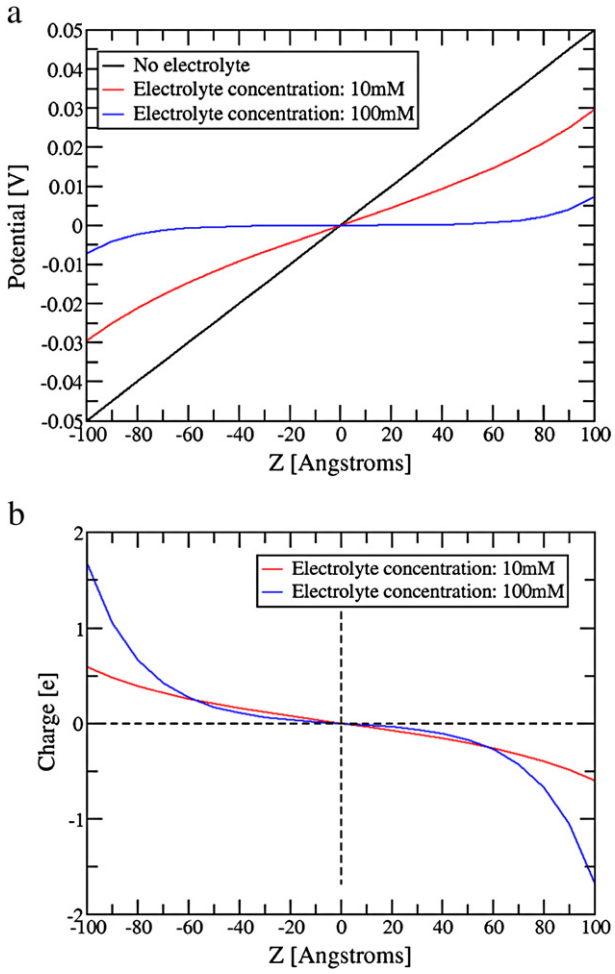

Fig. 5. (a) The electrolyte potential (in Volt) and (b) the electrolyte charge distribution along Z-axis for a system with two electrodes (external potential 100 mV). We have shown the results for two different electrolyte concentrations: 10 mM (red) and 100 mM (blue). Fig. 5(a) also shows the linear electrode potential (in absence of electrolyte) as reference (black). These calculations have been performed with (17X17) periodic images in the XY plane (see Fig. 7 for convergence study).

results are normalized with n_{bulk} rather than by Eq. (27). The PB treatment leads to results where the charge distribution is not conserved on the left side (or the right side) of the membrane. This creates a conceptual problem, since the initial conditions and the constraint in the short time before the ions pass through the membrane or a membrane channel, correspond to an electroneutral solution on each side of the membrane (zero net charge on each side). It is, of course, very likely that the accumulated positive charge next to the left side of the membrane is balanced by negative charges in the bulk or near the electrode (on the left side), and the neglect of the explicit charge near the electrode in the PB treatment does not change the PB results near the membrane. However, the formulation used in calculations of the capacity (where the capacity charges is evaluated in the PB treatment by integrating the charge on the left side of the membrane from minus infinity [40]), is formally problematic, since this charge is zero in the complete treatment of the system. The relationship between our treatment that keeps explicit counts of the ions and the PB treatment needs clearly a further study. However, it seems to us that the PB treatment does not look at the ions in the bulk or near the electrode as explicit ions that should be combined with the ions near the membrane when considering the specific charge balance on each side of the membrane. Thus the PB approach considers the electrolytes that move to the electrode in the same way that one would consider the electrons in the electric wires (namely does not consider them explicitly). We believe that looking at the electrolytes that balance the charge migration toward the membrane can provide an interesting time dependent insight.

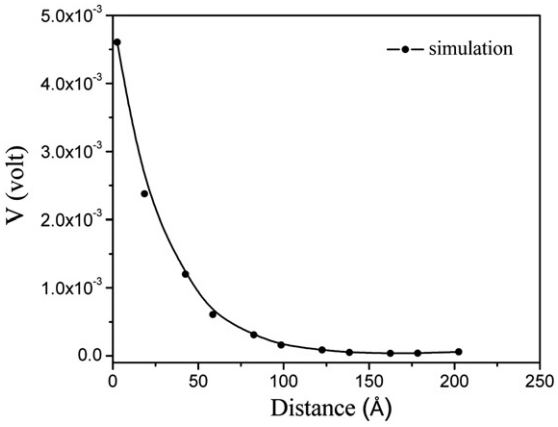

Fig. 4. The Gouy–Chapman potential.

An important requirement for the validation of our (or any other) model is the ability to reproduce the capacitance of the membrane system. Examining the performance of the present model we found out that the computed capacitance of our membrane system agrees

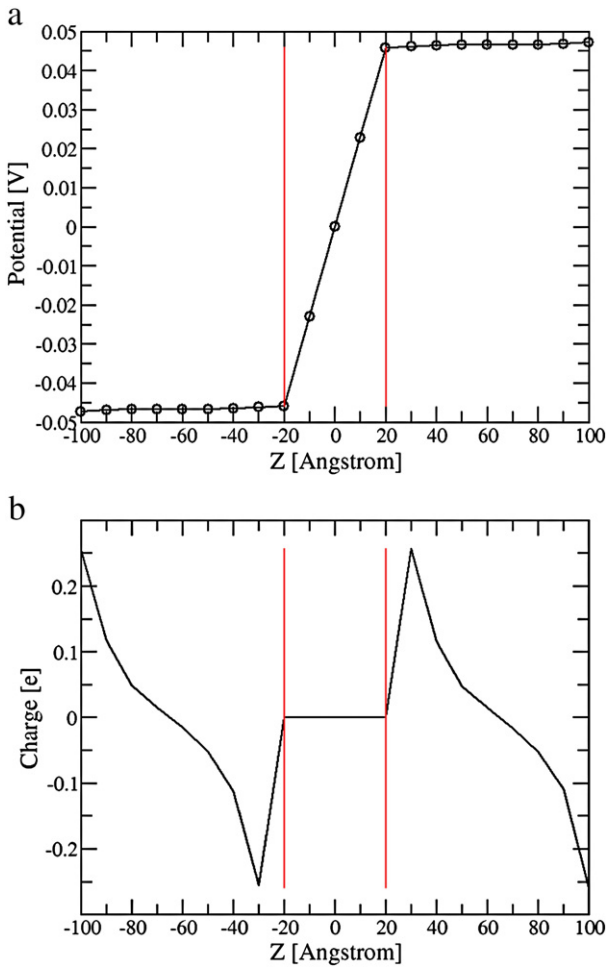

Fig. 6. (a) The electrostatic potential (in kcal/mol) and (b) electrolyte charge distribution along Z-axis for a system with two electrodes (external potential 100 mV), 40 A thick membrane at the center of the box (marked by red vertical lines) and electrolyte with concentration 100 mM. For schematic diagram of the system see Fig. 2. The present case required the use of (17×17) periodic images (in the XY plane) to reach convergence. For this system, the computed capacitance is 2.2×10^{-3} $CV^{-1}m^{-2}$ and the analytical capacitance is 4.3×10^{-3} $CV^{-1}m^{-2}$ [40].

quite well with the corresponding analytical expression of Lauger [40]. For example the system described in Fig. 6, the computed capacitance is 2.2×10^{-3} $CV^{-1}m^{-2}$, whereas the analytical estimate is 4.3×10^{-3} $CV^{-1}m^{-2}$ [40].

Another useful analysis is presented in Fig. 7, where we consider the convergence of the calculations with the number of replica cells. Here we must note the difference between the two types of electrodes models that we have implemented in our study. Namely, (i) the explicit electrode with finite size where the charge is assigned to every electrode grid point and (ii) the continuum electrode ($\mathbf{D_0}$ approach) as described above in Eqs. (30)–(34). Evidently the continuum electrode corresponds to an infinite electrode and Fig. 7 confirms that the electrode potential due to the explicit electrode converges to the linear form of the continuum electrode at the limit of large number of periodic images (17×17 in the XY plane). We have also shown that in presence of the electrolyte, the difference between these two approaches become lower and we obtained practical convergence by using 17×17 periodic images. It is instructive to note that for the explicit electrodes the potential across the simulation box increases with increasing number of images, whereas for the continuum $\mathbf{D_0}$ approach it decreases. This reflects the fact that a considerable part of the infinite electrode, in the $\mathbf{D_0}$ approach, exerts an unscreened potential on the grid points, which is higher than the corresponding value when an infinite box of electrolyte is present.

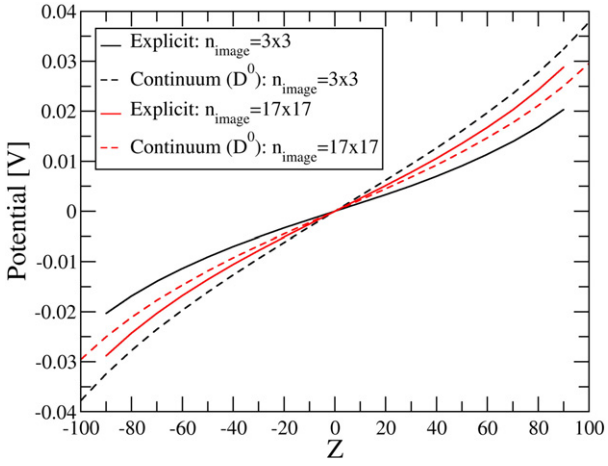

Fig. 7. The convergence of the electrolyte potential (in Volt) with increasing number of periodic images (see Section 2.2 for details about construction of the images) for a system with two electrodes (external potential 100 mV) and electrolyte solution (10 mM). Here we have checked the convergence for two different representations of the electrode system as described in Section 2.3, namely: (i) Explicit electrodes: where the electrodes are finite grid of point charges as given by Eq. 36 (solid line), and (ii) Continuum electrodes using D0 as given by Eq. 34 (dashed line). Electrolyte potential for each system has been computed for two different numbers of periodic images in XY plane: 3X3 (black) and 17X17 (red). The difference between the electrolyte potential obtained by explicit and continuum representations of electrode potential is large for fewer images (3X3: black lines), but they become almost identical at the limit of large number of images (17X17: red lines). Note that with increasing number of images the potential gets enhanced for the explicit electrodes, whereas it gets suppressed for the continuum electrodes due to the screening issues discussed in Section 2.3.

Thus we consider the explicit electrode to be a more consistent approach that correctly captures the behavior of the system at different finite sizes (where we can progressively increase the size and examine the overall convergence).

Next we consider the effect of moving charges in the membrane region, as a preparation for exploring the corresponding displacement charges in Kv1.2. This was done by first applying an external voltage of 0.1 V, placing a charge of +16e near the surface of the membrane (at the coordinate (0, 0,−10)) and letting the electrolytes equilibrate separately at each side ($Z<0$ and $Z>0$) without any transfer across the membrane. Subsequently we moved the charge (+16e) to the other side of the membrane (at the coordinate (0, 0, 10)) and let the electrolytes equilibrate in the same way as before. We define the gating charge as the change in the accumulated electrolyte charges, on either side of the membrane, upon movement of the (protein) charge inside the membrane (a more quantitative definition will be given in Eq. (42)). The computed results for such a system is described in Fig. 9 and the gating charge for the described conditions are found to be ~5.

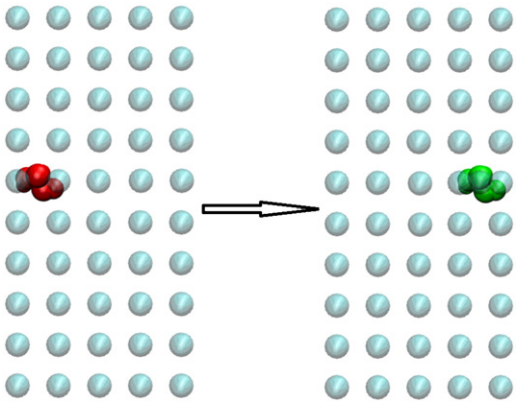

Fig. 8. A simplified model for exploring the gating charges. The model involves a membrane and positive charges that are moved from one side to the other.

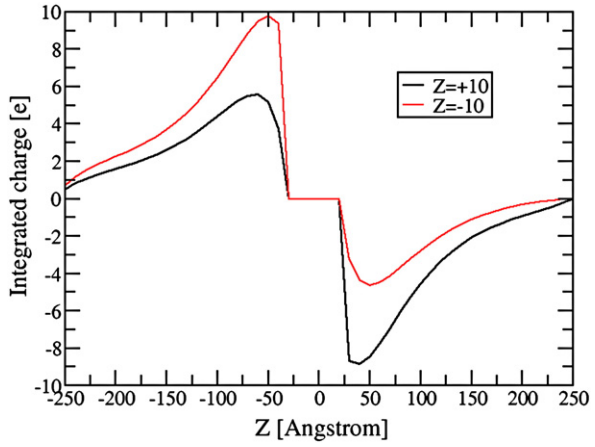

Fig. 9. The accumulative integration of the charge profiles for the model system described in Fig. 8 when the +16e charge resides at Z = +10 (black) and Z = -10 (red). Here we define the gating charge as the change in the accumulated electrolyte charges (the difference of the maxima in this figure), on either side of the membrane, upon movement of the (protein) charge inside the membrane (see Eq. 42). The gating charge for this system is found to be ~5.

3.2. Treating the bulk in studies of membrane potential

As stated in Section 2.2 we would like to have the option to represent a part of the electrolyte system, where the potential is constant, by a "bulk region", in order to enhance computational efficiency. To justify this treatment we start with the system described in Fig. 10(a) and try to reach equivalence with the system of Fig. 10 (b). In Fig 10(a) we schematically describe a very large system, where all grid points in the shaded regions (II and IV) are very far away from both electrode and membrane surfaces. The shaded regions, which will become the bulk regions are much larger compared to the other regions. The computed electrolyte potential on these grid points are constant (−V/2 and +V/2 for regions II and IV, respectively) and the corresponding net charges are equal to zero. Under this condition, we can easily implement a separation of the bulk grid points from the explicit electrolyte system, and thus avoid computing the energy and charges of the bulk grid points during the iterations. The above separation has been schematically described in Fig. 10(b), where we separate regions II and IV from the explicit system, and these regions coalesce into two planes at Z_B^L and Z_B^R, respectively. Note that in this treatment we take into account of the width of the bulk ($\Delta Z_B = Z_B^{(2)} - Z_B^{(1)} = Z_B^{(4)} - Z_B^{(3)}$) appropriately, both in the computation of the electrode potential and the evaluation of the interaction between the grid points. In computing the electrode (external) potential on the *i*th grid point we modify Eq. (34) and use:

$$
\begin{aligned}
V_{ext}^i &= D_Z^0(Z_i - Z_0)/\bar{\varepsilon}_{wat}, \text{ when } Z_i \le Z_B^L \\
V_{ext}^i &= D_Z^0/\bar{\varepsilon}_{loc}(Z_i - Z_0 + \Delta Z_B), \text{ when } Z_B^L < Z_i < Z_1 \\
V_{ext}^i &= D_Z^0(Z_1 - Z_0 + \Delta Z_B)/\bar{\varepsilon}_{wat} + D_Z^0/\bar{\varepsilon}_{loc}(Z_i - Z_1), \text{ when } Z_1 \le Z_i \le Z_2 \\
V_{ext}^i &= D_Z^0(Z_1 - Z_0 + \Delta Z_B)/\bar{\varepsilon}_{wat} + D_Z^0(Z_2 - Z_1)/\bar{\varepsilon}_{loc} + D_Z^0(Z_i - Z_2)/\bar{\varepsilon}_{wat}, \text{ when } Z_2 < Z_i < Z_B^R \\
V_{ext}^i &= D_Z^0(Z_1 - Z_0 + \Delta Z_B)/\bar{\varepsilon}_{wat} + D_Z^0(Z_2 - Z_1)/\bar{\varepsilon}_{loc} + D_Z^0(Z_i - Z_2 + \Delta Z_B)/\bar{\varepsilon}_{wat}, \text{ when } Z_i \ge Z_B^R
\end{aligned}
\tag{38}
$$

This modified external potential for a system with a virtual bulk is shown in Fig. 11. Obviously, we need to modify the distance between two grid points *i* and *j* appropriately when they belong to different sides of a bulk boundary.

Now that we have a fraction of grid points in our system with constant potential, we can rewrite the normalization constant of Eq. (20) as:

$$A^{\pm} = \sum_i e^{\mp\beta\phi_i} = \sum_{i\in box} e^{\mp\beta\phi_i} + N_{bulk}^{grid} e^{\mp\beta\phi_{bulk}} \tag{39}$$

where, the summation in the first term runs over all the grid points treated explicitly in the simulation box, while N_{bulk}^{grid} grid points are considered as a part of a "virtual bulk", using $N_{system}^{grid} = N_{box}^{grid} + N_{bulk}^{grid}$. Here, N_{bulk}^{grid} is computed using $N_{bulk}^{grid} = N_{XY}\Delta Z_B$ as the bulk dimension, where N_{XY} is the number of grid points on every grid surface on the XY plane.

Note that in the above treatment we compute the bulk potential on the fly at every iteration, taking this potential as the potential at the bulk plane $Z = Z_B^L$ for the smaller system of Fig. 10(b). This approach is valid as long as the computed potential ($V(Z)$) converges to a

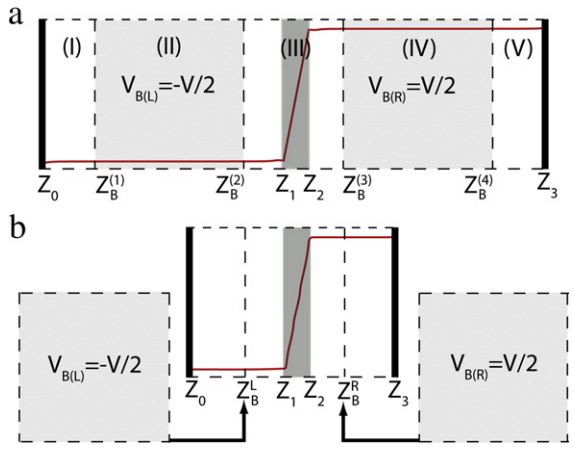

Fig. 10. A schematic diagram for the treatment of the bulk regions: (a) fully explicit system with very large dimensions, (b) the corresponding smaller system with regions (II) and (IV) separated out and marked as "bulk regions" that have constant electrolyte potential (VB) and zero net charge. Regions (II) and (IV) of system (a) coalesce into the planes and in system (b). The red lines indicate the computed electrolyte potential for respective systems (also see Fig. 11).

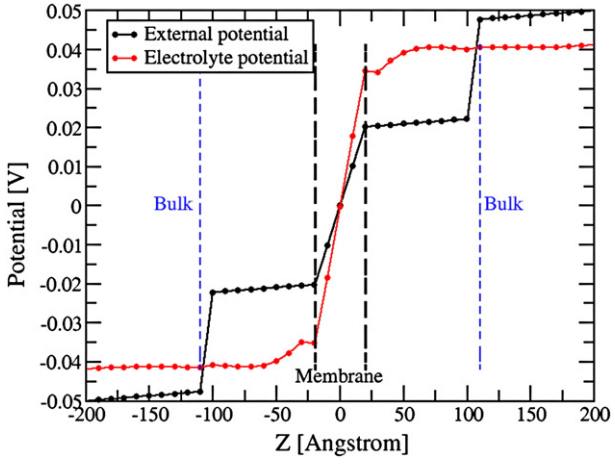

Fig. 11. Validation of the treatment of the virtual bulk regions. The black line shows the external electrode potential as obtained using Eq. 38. Note that the electrode potential is obtained by integrating D^0 across the bulk dimension, so it is discontinuous across the planes and of Fig. 10(b) as marked in blue here. But the electrolyte potential (marked in red) is continuous and constant across the bulk regions with the value being equal to the bulk potential VB. This validates the consistency of treating the bulk grid points separately with constants potential and zero net charge. The membrane region (thickness 40Å) has been marked by parallel dashed lines at Z = -20 and Z = +20.

complete plateau across the planes at Z_B^L and Z_B^R for the smaller system, i.e. we must satisfy the conditions:

$$\left(\frac{dV}{dZ}\right)_{Z=Z_B^L} = \left(\frac{dV}{dZ}\right)_{Z=Z_B^R} = 0 \qquad Q_{Z=Z_B^L} = Q_{Z=Z_B^R} = 0 \tag{40}$$

In this way we reach a correspondence between the model with a virtual bulk (Fig. 10(b)) and the model where the bulk region is treated explicitly (Fig. 10(a)). The validation results of our treatment of a virtual bulk are presented in Fig. 11.

3.3. A preliminary evaluation of the potential in the Kv1.2/membrane system

The CG model developed in this work has been motivated in part by the challenge of exploring the effect of an external potential on the Kv1.2 voltage activated channel. Thus we, obviously, would like to use our model in exploring this important system. However, considering the fact that this is primarily a method development paper we leave the careful analysis of voltage activated channels to subsequent works and only provide here illustrations of the capacity of our model. Our illustrative study examined the Kv1.2 by considering the open and closed models of the protein/membrane system. Considering the tentative nature of our study, we have used the atomistic structural model built using Rosetta and used by Pathak et al. [67] for both the open and closed structures.

We started by taking the tentative closed structure in the membrane electrolyte system (Fig. 12), under zero external potential, and determining the ionization state (protonation state) of the protein ionizable groups using the CG model and the MC time dependent constant pH simulation approach [30]. We have also neutralized the protein charges (Q_p) by adjusting the electrolyte distribution (replacing in Eq. (25) ($Q^+_{box}+Q^+_{bulk}$) by ($Q^+_{box}+Q^+_{bulk}$) − Q_p, and of course, allowing the electrolytes to equilibrate. Next we change the external potential to 0.1 mV and let the electrolyte equilibrate separately at each side of the membrane). Next we obtain the electrostatic potential and the electrolyte charge distribution for the closed channel and the corresponding results are presented in Fig. 13. We have also repeated the same calculations for the open structure (Fig. 13), allowing the same full equilibration (note that this procedure is not the one that will be used below for evaluating the gating charge). At this stage we only want to note that we can reproduce reasonably behaving potential profiles and that the potential in the membrane region can be used in calculating the gating charge (see below).

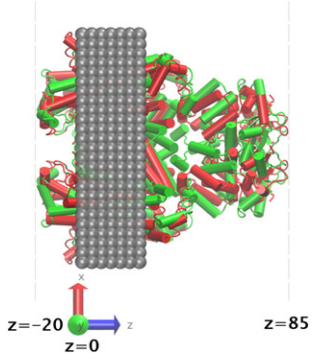

Fig. 12. Molecular representation of the Kv1.2 channel system in open (red) and closed green conformations.

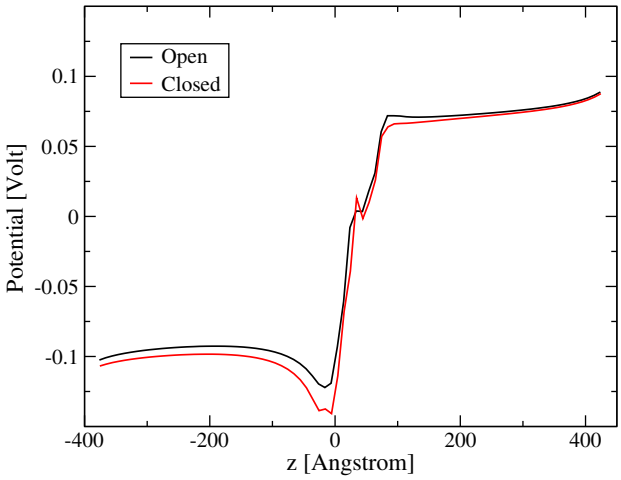

Fig. 13. The total electrostatic potential in the Kv1.2 system for the open (in red) and closed (in black) conformations.

3.4. The gating charge

The gating charge is a crucial parameter that reflects the response of the system following the application of the external potential but before the ions are allowed to pass through the channel [1]. The evaluation (and operational definition) of the gating charge is almost always done in an indirect way, using reasonable but not necessarily microscopic assumptions. That is, one may simply determine the fraction of open and closed channels as a function of the applied potential and ask what is the Boltzmann probability for the voltage induced structural change [1]. Basically this is equivalent to the assumption that the energy needed to move the gating charge, Q_{gate}, in the membrane electric field is equal to the work of moving the protein charges between the two configurations, under the membrane electric field. This assumption leads to the expression [1,68]:

$$Q_{gate}\Delta V = \Delta G^{cl\to op} \tag{41}$$

where $\Delta G^{cl\to op}$ is the free energy contribution of the membrane potential for moving from the closed to open configuration and ΔV is the change in the electrostatic potential between the initial and final position of the protein effective charge, and where the practical determination of Q_{gate} is done by considering the conductance/voltage curve at low probability of having an open state up to the limiting potential where Q(V) reach a plateau (see ref. 70). The problem with the use of eq. (41), or related treatments, is that the membrane potential is assumed to be linear across the membrane with identical value for each X,Y that corresponds to a given Z value (for this assumption see also ref 20). This is likely to be a reasonable approximation and it has been used in previous macroscopic studies [67,68]. Obviously, such a picture would be justified if the potential across the protein/ membrane system was obtained by converging microscopic simulations. However, in such cases it is unlikely that we will have the same potential in different sites with the same Z value. Thus such a treatment does not really provide a microscopic description even if a few of the relevant quantities (e.g. the average displacements) are evaluated microscopically [20]. A more microscopic strategy (terms G-route in ref. [20]) involves calculating the free energy change associated with each residue in the two configurations under the effect of the external potential. This approach does provide a fully microscopic treatment of the effect of the potential on the protein. However, it is not clear how accurate is the corresponding G-route free energy treatment, since the convergence of applying such procedure to voltage effects has never been established by reproducing well defined observed effects (namely pK_a

changes, redox changes or spectral shifts). One major challenge involves the ability to capture the equilibration of the electrolytes by microscopic calculations. Furthermore, calculating charging free energies at different sites (e.g. after and before the conformational change) is extremely challenging as has been demonstrated in our studies of pK_a in non-polar protein interiors [69]. Finally, although equating the calculated free energy to the product of Q_{gate} and ΔV is very reasonable, it still does not constitute actual calculation of a gating charge. More specifically, while it is true that is a real observable (obtained from the Q-V curve [70]), Q_{gate} of Eq. (41) may not correspond to the integral of the gating current at the limiting potential. Thus we like to focus of the actual measured Q_{gate} and in doing so we assume that the gating current is due to the motion and accumulation of the electrolyte charges. The challenge is of course to get the observed integrated current and the corresponding gating charge.

This challenge is met here by first applying an initial potential in the closed structure, letting the electrolytes equilibrate in this structure and then fixing the number of positive and negative ions on both side of the membrane. Next we apply a new potential and change the protein structure from its closed to the open conformation, while allowing the electrolytes to equilibrate locally, with the constraint that they cannot pass through the channel.

In calculating the gating charge, we note that the movement of the positively charged protein residues to the Z direction leads to movement of negative solution ions toward the membrane protein system (this polarization is clearly captured by the PB treatments). However, the measured current is actually due to the movement of the compensating positively charged ions toward the electrode green. Of course, this current is the same (with opposite sign) as the opposite negative current that moved towards the membrane, but the physics is better described by considering the actual gating current measured for example in the work of ref 70. Thus we evaluate the gating charges by

$$Q_{gate} = \int_0^t (\Delta q/\Delta t)\, dt = \int_{-\infty}^{Z'} \left(\Delta q_{grid}/\Delta Z\right) dZ \qquad (42)$$

where the first integral is related to the gating current (at the limiting potential) and the second integral evaluates the charges generated upon complete structural change, by the current after the current equilibrates in the left side but before it penetrates the membrane. Z' is the point to the left of Z_1 where the accumulated charge distribution near the membrane has decayed to zero. The computed charge

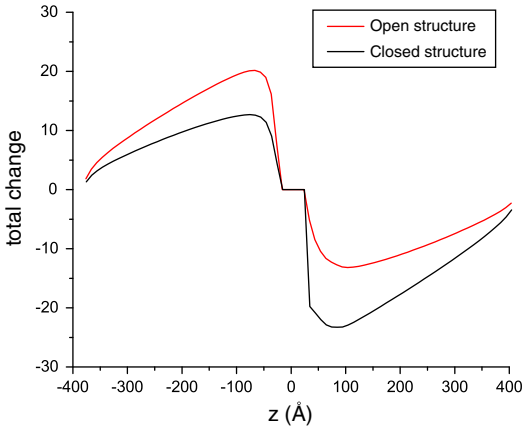

Fig. 14. Electrolyte charge profiles for the open and closed conformations, where we do not allow for ion equilibration (transfer of ions through the membrane) and where we have allowed the protein ionization states to change while moving between the two structures. The integral of this profile (see Eq. (42)) gives us the estimate of gating charge.

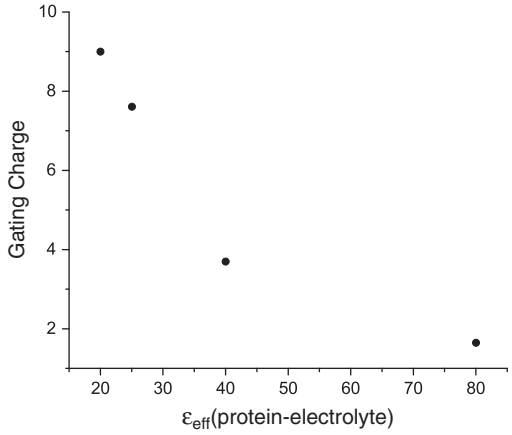

Fig. 15. Gating charge as a function of dielectric constant between protein and electrolyte.

distributions ($\Delta q_{grid}(Z)$) for both the open and closed channels are shown in Fig.14.

One of the most interesting aspects of the present study was the finding that the protein ionization states change significantly between the open and closed structures, and that this change can play a significant role in establishing the correct gating charge, which is a factor that has not been considered in other studies. With our ability to model time-dependent proton transfer process [26] it would be very exciting to find out the realistic ionization states and the corresponding gating charge. This issue will be considered in further detail in our subsequent studies.

The value of the gating charge appears to depend on the dielectric used for the interaction between the electrolytes and the protein charges and the corresponding dependence is described in Fig. 15. For example, the gating charge evaluated by Eq. (42) changed from 2 to 9 upon change of the above dielectric from 80 to 20. We note here that the experimentally observed gating charge for the Shaker and Kv2.1 K^+ channel is 3 to 4 charge units per voltage sensor (i.e. 12 to 16 charges per channel) [71] and this value is obtained in our calculation with an effective dielectric constant below 15. However, we leave a deeper analysis of our finding to a subsequent work.

The current model can become even more physical if we actually make it time-dependent. This can be done by running LD on the CG model and allowing the protein to move (within the given time) and also allow for time-dependent proton transfer between the protein groups and the solution. At the same time we may be able to assume (after proper validation) that the electrolyte equilibration is much faster than the protein conformational change. Under this condition we should be able to obtain fluctuating polarization charges that can be related to the observed gating current.

3.5. The energetics of ion channel systems

The present model can be used to explore the overall energetics of the open and closed structures. These challenging calculations are expected to give interesting information at least on a qualitative level, since the CG model has performed quite well in studies of protein stability [30] and in exploring some issues about the insertion of membrane proteins [27]. Our ability to properly simulate the ionization states and their changes with the structure of the protein and the external potential, is a key advance over most other related models of voltage activate channels. For example, we should be able to examine the nature of the conserved acidic and basic side chains in the voltage-sensing domains of internal salt-bridge networks whose ionization state may be state-dependent. We can also examine the role of the interaction between the basic side chains in the voltage-

sensing domains and the lipid phosphates (see ref. [71]), since these interactions have been shown to be indispensable for channel function (see ref. [72]).

Despite the great interest in the energetics of the Kv1.2 channel, we focus in this paper on the methodological issues and we prefer to leave the analysis of the energetics to a subsequent study. Nevertheless, our point is that in view of the enormous difficulties in obtaining the energetics of the closed to open structural transition in voltage activated channels we see a great potential in the use of our CG model.

4. Concluding remarks

The molecular origin of voltage activated channels is a subject of major current interest. Yet, using non-phenomenological models to correlate the available structural models with the activation of channels by external potential has not elucidated the energetics of such processes. Furthermore, the description of the effect of external potential on membrane proteins has not reached the stage where it provides a clear physical picture. That is, while continuum studies of the potential and electrolytes near the membrane have been very useful [39,40,73,74], the description of the electrolytes far away from the membrane and near the electrodes has not been considered explicitly. Furthermore, the assumed dielectric in the membrane-protein system has not been validated. Microscopic and semimicroscopic attempts to describe the potential and electrolytes have provided some interesting hints, but at least as much as the electrolytes are concerned we clearly have not reached at a stage with a clear quantitative understanding. The situation is better when one restricts himself to modeling electrolytes in DH and GC type of problems, where MC models have been very instrumental [44,59], but such studies have not been extended (to the best of our knowledge), to the description of membrane potential and in particular to voltage-activated channels.

This work developed a CG model for studies of the effect of external potentials on membrane proteins and tried to explore the utility of CG modeling in simulating general effects of membrane potentials on membrane proteins and related systems. The model developed here involves our early CG model of protein membrane systems and a newly developed model of the electrolyte solution and the effect of the external potential due to electrodes. The electrolyte model allows us to navigate between the more microscopic MC modeling and the faster mean field models and helps in providing some insight on various aspects that are needed in order to understand the nature of the effect of external potentials.

Our model was applied for several well defined test cases (e.g. the DH and GC models) as well as to the nature of the potential and charge distribution between two electrodes. It was then used in studies of membrane systems, reproducing the expected capacity and shading a new light on the nature of the electrolyte charge distribution. We have also explored the trend in gating charge in a simple model with electrodes/membrane and internal membrane charges.

After the validation studies we have performed preliminary simulations of the Kv1.2 channel, evaluating the membrane potential and the gating charge. This was done, however, in a non-standard and challenging way, looking on the change in the electrolyte charges rather than on the interaction between the linearized external potential and the protein charges. The calculations performed were given only as an illustrative example leaving more systematic and system specific simulations to a subsequent work, which is now in progress.

The new model should allow us to focus on key issues such as the nature and the effect of the dielectric in the protein–membrane system, and to move beyond the continuum assumptions. Further work is clearly needed including evaluation of the overall change in the protein energy. We also expect to be able to simulate the fluctuations in the gating current and other related effects.

Acknowledgements

We are grateful to Prof. Gren Patey, Prof. Chi Mac and Prof. Chris Miller. This work was supported by the National Science Foundation Grant MCB-0342276 and NIH grant GM40283. We acknowledge the University of Southern California's High Performance Computing and Communications Center for computer time.

References

[1] B. Hille, Ion Channels of Excitable Membranes, 3rd ed. Sinauer Assoc., Sunderland, MA, 2001.
[2] G. Eisenman, R. Horn, Ionic selectivity revisted: the role of kinetic and equilibrium processes in ion permeation through channels, J. Membr. Biol. 50 (1983) 1025–1034.
[3] D.A. Doyle, J.M. Cabral, R.A. Pfuetzner, A.L. Kuo, J.M. Gulbis, S.L. Cohen, B.T. Chait, R. MacKinnon, The structure of the potassium channel: molecular basis of K^+ conduction and selectivity, Science 280 (1998) 69–77.
[4] S.B. Long, E.B. Campbell, R. MacKinnon, Crystal structure of a mammalian voltage-dependent Shaker family K^+ channel, Science 309 (2005) 897–903.
[5] J. Rettig, S.H. Heinemann, F. Wunder, C. Lorra, D.N. Parcej, J.O. Dolly, O. Pongs, Inactivation properties of voltage-gated K^+ channels altered by presence of beta-subunit, Nature 369 (1994) 289–294.
[6] W.A. Catterall, Structure and function of voltage-gated ion channels, Annu. Rev. Biochem. 64 (1995) 493–531.
[7] N.B. Yang, A.L. George, R. Horn, Molecular basis of charge movement in voltage-gated sodium channels, Neuron 16 (1996) 113–122.
[8] A. Cha, G.E. Snyder, P.R. Selvin, F. Bezanilla, Atomic scale movement of the voltage-sensing region in a potassium channel measured via spectroscopy, Nature 402 (1999) 809–813.
[9] P. Lauger, Ion transport through pores: a rate-theory analysis, Biochim. Biophys. Acta 311 (1973) 423.
[10] J.H. Morals-Cabral, Y. Zhou, R. MacKinnon, Energetic optimization of ion conduction rate by the K^+ selectivity filter, Nature 414 (2001) 37–42.
[11] A. Burykin, M. Kato, A. Warshel, Exploring the origin of the ion selectivity of the KcsA potassium channel, Proteins 52 (2003) 412–426.
[12] S. Berneche, B. Roux, Molecular dynamics of the KcsA K+ channel in a bilayer membrane, Biophys. J. 78 (2000) 2900–2917.
[13] I.H. Shrivastava, M.S.P. Sansom, Simulations of ion permeation through a potassium channel: molecular dynamics of KcsA in a phospholipid bilayer, Biophys. J. 78 (2000) 557–570.
[14] V. Luzhkov, J. Aqvist, K^+/Na^+ selectivity of the KcsA potassium channel from microscopic free energy perturbation calculations, Biochim. Biophys. Acta 36446 (2001) 1–9.
[15] J. Åqvist, V. Luzhkov, Ion permeation mechanism of the potassium channel, Nature 404 (2000) 881–884.
[16] S. Berneche, B. Roux, Energetics of ion conduction through the K^+ channel, Nature 414 (2001) 73–77.
[17] A. Burykin, C.N. Schutz, J. Villa, A. Warshel, Simulations of ion current in realistic models of ion channels: the KcsA potassium channel, Proteins: Struct. Funct. Genet. 47 (2002) 265–280.
[18] D. Boda, D.D. Busath, D. Henderson, S. Sokolowski, Monte Carlo simulations of the mechanism for channel selectivity: the competition between volume exclusion and charge neutrality, J. Phys. Chem. B 104 (2000) 8903–8910.
[19] D.P. Tieleman, P.C. Biggin, G.R. Smith, M.S.P. Sansom, Simulation approaches to ion channel structure -function relationships, Q. Rev. Biophys. 34 (2001) 473–561.
[20] F. Khalili-Araghi, V. Jogini, V. Yarov-Yarovoy, E. Tajkhorshid, B. Roux, K. Schulten, Calculation of the gating charge for the Kv1.2 voltage-activated potassium channel, Biophys. J. 98 (2010) 2189–2198.
[21] B. Roux, The Membrane Potential and its Representation by a Constant Electric Field in Computer Simulations, Biophys. J. 95 (2008) 4205–4216.
[22] J.A. Freites, D.J. Tobias, S.H. White, A voltage-sensor water pore, Biophys. J. 91 (2006) L90–L92.
[23] M. Grabe, H. Lecar, Y.N. Jan, L.Y. Jan, A quantitative assessment of models for voltage-dependent gating of ion channels, Proc. Natl. Acad. Sci. U.S.A. 101 (2004) 17640–17645.
[24] A. Warshel, P.K. Sharma, M. Kato, W.W. Parson, Modeling electrostatic effects in proteins, Biochim. Biophys. Acta 1764 (2006) 1647–1676.
[25] S. Kamerlin, S. Vicatos, A. Dryga, A. Warshel, Coarse-Grained (Multiscale) Simulations in Studies of Biophysical and Chemical Systems, Annu. Rev. 62 (2010) 41–64.
[26] B.M. Messer, M. Roca, Z.T. Chu, S. Vicatos, A.V. Kilshtain, A. Warshel, Multiscale simulations of protein landscapes: using coarse-grained models as reference potentials to full explicit models, Proteins 78 (2010) 1212–1227.
[27] A. Rychkova, S. Vicatos, A. Warshel, On the energetics of translocon-assisted insertion of charged transmembrane helices into membranes, Proc. Natl. Acad. Sci. U.S.A. 107 (2010) 17598–17603.
[28] M. Roca, B. Messer, A. Warshel, Electrostatic contributions to protein stability and folding energy, FEBS Lett. 581 (2007) 2065–2071.
[29] A. Warshel, P.K. Sharma, M. Kato, W.W. Parson, Modeling electrostatic effects in proteins, Biochim. Biophys. Acta 1764 (2006) 1647–1676.
[30] S. Vicatos, M. Roca, A. Warshel, Effective approach for calculations of absolute stability of proteins using focused dielectric constants, Proteins: Struct. Funct. Bioinform. 77 (2009) 670–684.

[31] A. Warshel, S.T. Russell, Calculations of electrostatic interactions in biological systems and in solutions, Q. Rev. Biophys. 17 (1984) 283–421.
[32] A. Warshel, S.T. Russell, A.K. Churg, Macroscopic models for studies of electrostatic interactions in proteins — limitations and applicability, Proc. Natl. Acad. Sci. U.S.A. 81 (1984) 4785–4789.
[33] S.C.L. Kamerlin, P.K. Sharma, Z.T. Chu, A. Warshel, Ketosteroid isomerase provides further support for the idea that enzymes work by electrostatic preorganization, Proc. Natl. Acad. Sci. U.S.A. 107 (2010) 4075–4080.
[34] J. Aqvist, A. Warshel, Energetics of ion permeation through membrane channels — solvation of Na^+ by gramicidin-A, Biophys. J. 56 (1989) 171–182.
[35] Z.Z. Fan, J.-K. Hwang, A. Warshel, Using simplified protein representation as a reference potential for all-atom calculations of folding free energy, Theor. Chem. Acc. 103 (1999) 77–80.
[36] A. Warshel, S.T. Russell, Calculations of electrostatic interactions in biological systems and in solutions, Q. Rev. Biophys. 17 (1984) 283–422.
[37] I. Vorobyov, T.W. Allen, The electrostatics of solvent and membrane interfaces and the role of electronic polarizability, J. Chem. Phys. 132 (2010).
[38] V. Luzhkov, A. Warshel, Microscopic models for quantum-mechanical calculations of chemical processes in solutions — LD/AMPAC and SCAAS/AMPAC calculations of solvation energies, J. Comput. Chem. 13 (1992) 199–213.
[39] C.T. Everitt, D.A. Haydon, Electrical capacitance of a lipid membrane separating 2 aqueous phases, J. Theor. Biol. 18 (1968) 371.
[40] P. Lauger, W. Lesslaue, E. Marti, J. Richter, Electrical properties of bimolecular phospholipid membranes, Biochim. Biophys. Acta 135 (1967) 20.
[41] I. Klapper, R. Hagstrom, R. Fine, K. Sharp, B. Honig, Focusing of electric fields in the active site of copper–zinc superoxide dismutase effects of ionic strength and amino acid modification, Proteins: Struct. Funct. Genet. 1 (1986) 47–59.
[42] S. McLaughlin, The electrostatic properties of membranes, Annu. Rev. Biophys. Biophys. Chem. 18 (1989) 113–136.
[43] B. Jonsson, H. Wennerstrom, B. Halle, Ion distributions in lamellar liquid-crystals — a comparison between results from Monte-Carlo simulations and solutions of the Poisson–Boltzmann equation, J. Phys. Chem. 84 (1980) 2179–2185.
[44] G.M. Torrie, J.P. Valleau, Electrical double-layers. 1. Monte-Carlo study of a uniformly charged surface, J. Chem. Phys. 73 (1980) 5807–5816.
[45] D. Henderson, D. Boda, Insights from theory and simulation on the electrical double layer, Phys. Chem. Chem. Phys. 11 (2009) 3822–3830.
[46] K. Kiyohara, K. Asaka, Monte Carlo simulation of electrolytes in the constant voltage ensemble, J. Chem. Phys. 126 (2007) 14.
[47] D. Boda, K.Y. Chan, D. Henderson, Monte Carlo simulation of an ion-dipole mixture as a model of an electrical double layer, J. Chem. Phys. 109 (1998) 7362–7371.
[48] A. Martin-Molina, C. Calero, J. Faraudo, M. Quesada-Perez, A. Travesset, R.H. Alvarez, The hydrophobic effect as a driving force for charge inversion in colloids, Soft Matter 5 (2009) 1350–1353.
[49] L. Pegado, B. Jonsson, H. Wennerstrom, Ion–ion correlation attraction in a molecular solvent, J. Chem. Phys. 129 (2008) 11.
[50] D. Boda, W.R. Fawcett, D. Henderson, S. Sokolowski, Monte Carlo, density functional theory, and Poisson–Boltzmann theory study of the structure of an electrolyte near an electrode, J. Chem. Phys. 116 (2002) 7170–7176.
[51] A.G. Moreira, R.R. Netz, Simulations of counterions at charged plates, Eur. Phys. J. E Soft Matter 8 (2002) 33–58.
[52] M. Yi, H. Nymeyer, H.X. Zhou, Test of the Gouy–Chapman theory for a charged lipid membrane against explicit-solvent molecular dynamics simulations, Phys. Rev. Lett. 101 (2008) 4.
[53] P. Beroza, D.R. Fredkin, M.Y. Okamura, G. Feher, Protonation of interacting residues in a protein by a Monte Carlo method: application to lysozyme and the photosynthetic reaction center of Rhodobacter sphaeroides, Proc. Natl. Acad. Sci. U.S.A. 88 (1991) 5804–5808.
[54] C. Tanford, R. Roxby, Interpretation of protein titration curves. Application to lysozyme, Biochemistry 11 (1972) 2192–2198.
[55] Y.Y. Sham, Z.T. Chu, A. Warshel, Consistent calculations of pK_a's of ionizable residues in proteins: semi-microscopic and microscopic approaches, J. Phys. Chem. B 101 (1997) 4458–4472.
[56] F.S. Lee, Z.T. Chu, A. Warshel, Microscopic and semimicroscopic calculations of electrostatic energies in proteins by the POLARIS and ENZYMIX programs, J. Comput. Chem. 14 (1993) 161–185.
[57] B.J. Klein, G.R. Pack, Calculations of the spatial-distribution of charge-density in the environment of DNA, Biopolymers 22 (1983) 2331–2352.
[58] G.M. Torrie, J.P. Valleau, Electrical double-layers. 1. Monte-Carlo study of a uniformly charged surface, J. Chem. Phys. 73 (1980) 5807–5816.
[59] G.M. Torrie, J.P. Valleau, G.N. Patey, Electrical double-layers. 2. Monte-Carlo and HNC studies of image effects, J. Chem. Phys. 76 (1982) 4615–4622.
[60] B. Roux, Influence of the membrane potential on the free energy of an intrinsic protein, Biophys. J. 73 (1997) 2980–2989.
[61] D.P. Tieleman, H.J.C. Berendsen, M.S.P. Sansom, Voltage-dependent insertion of alamethicin at phospholipid/water and octane/water interfaces, Biophys. J. 80 (2001) 331–346.
[62] H. Lecar, H.P. Larsson, M. Grabe, Electrostatic model of S4 motion in voltage-gated ion channels, Biophys. J. 85 (2003) 2854–2864.
[63] M. Grabe, H.C. Lai, M. Jain, Y.N. Jan, L.Y. Jan, Structure prediction for the down state of a potassium channel voltage sensor, Nature 445 (2007) 550–553.
[64] J.D. Jackson, Classical Electrodynamics, 3rd ed. John Wiley & Sons, Inc., New York, 1999.
[65] E.M. Purcell, Electricity and Magnetism, McGraw-Hill Book Company, 1965.
[66] M. Gouy, J. Phys. Theor. Appl. 9 (1910) 457.
[67] M.M. Pathak, V. Yarov-Yarovoy, G. Agarwal, B. Roux, P. Barth, S. Kohout, F. Tombola, E.Y. Isacoff, Closing in on the resting state of the shaker K^+ channel, Neuron 56 (2007) 124–140.
[68] M. Grabe, H. Lecar, Y.N. Jan, L.Y. Jan, A quantitative assessment of models for voltage-dependent gating of ion channels, Proc. Natl. Acad. Sci. U.S.A. 101 (2004) 17640–17645.
[69] M. Kato, A. Warshel, Using a charging coordinate in studies of ionization induced partial unfolding, J. Phys. Chem. B 110 (2006) 11566–11570.
[70] S.A. Seoh, D. Sigg, D.M. Papazian, F. Bezanilla, Voltage-sensing residues in the S2 and S4 segments of the Shaker K^+ channel, Neuron 16 (1996) 1159–1167.
[71] S.B. Long, X. Tao, E.B. Campbell, R. MacKinnon, Atomic structure of a voltage-dependent K^+ channel in a lipid membrane-like environment, Nature 450 (2007) 376–382.
[72] D. Schmidt, Q.-X. Jiang, R. MacKinnon, Phospholipids and the origin of cationic gating charges in voltage sensors, Nature 444 (2006) 775–779.
[73] B. Farrell, C. Do Shope, W.E. Brownell, Voltage-dependent capacitance of human embryonic kidney cells, Phys. Rev. E 73 (2006) 17.
[74] A.H. Hainsworth, S.B. Hladky, Effects of double-layer polarization on ion-transport, Biophys. J. 51 (1987) 27–36.
[75] J. Florian, A. Warshel, ChemSol, University of Southern California, Los Angeles, 1999.

Further Reading

[1] A. Warshel, A. Dryga, Simulating Electrostatic Energies in Proteins; Perspectives and Some Recent Studies of pKas, Redox and other crucial functional properties, Proteins 79 (2011) 3469–3484.
[2] A. Warshel, P.K. Sharma, M. Kato, W.W. Parson, Modeling electrostatic effects in proteins, Biochim. Biophys. Acta 1764 (2006) 1647–1676.